# New generation of tuning forks for quartz-enhanced photoacoustic spectroscopy

P. Patimisco[a], A. Sampaolo[a], M. Giglio[a], S. dello Russo[a], A. Elefante[a], G. Menduni[a,b], V. Passaro[b], H. Rossmadl[c], V. Mackowiak[c], Bruno Gross[c], Alex Cable[d], F. K. Tittel[e], and V. Spagnolo[a]

[a] PolySense Lab - Dipartimento Interateneo di Fisica, University and Politecnico of Bari, Via Amendola 173, Bari, Italy
[b]Photonics Research Group, Dipartimento di Ingegneria Elettrica e dell'informazione, Politecnico di Bari, Via Orabona 4, Bari, 70126, Italy
[c]Thorlabs GmbH, Hans-Boeckler-Straße 6, 85221 Dachau, Germany
[d]Thorlabs, Inc., 56 Sparta Ave., Newton, 07860, USA
[e]Department of Electrical and Computer Engineering, Rice University, 6100 Main Street, Houston, TX 77005, USA

## ABSTRACT

We report on the performance of new quartz tuning fork (QTF) designs optimized for quartz-enhanced photoacoustic spectroscopy (QEPAS). We investigated the impact on resonance properties of prong geometries differing from the standard rectangular one. We proposed a QTF with T-shaped prongs and a QTF with prongs having rectangular grooves carved on the surface. QTFs were implemented in a QEPAS sensor and performances were compared in terms of signal-to-noise ratio (SNR). Then, QTFs were acoustically coupled with single- and dual-tube micro-resonator systems. A record x60 SNR enhancement factor with respect to the bare QTF was achieved with QTF having T-shaped prongs.

**Keywords:** quartz-enhanced photoacoustic spectroscopy, gas sensing, tuning fork, quantum cascade laser.

## 1. INTRODUCTION

Quartz tuning forks (QTFs) have shown a huge potential as pressure waves transducers in quartz-enhanced photoacoustic spectroscopy (QEPAS) for gas sensing applications [1-6]. The resonance properties of the QTF mainly determine the performance of a QEPAS sensor [7-11]. Since its introduction in 2002 and for more than 10 years later, standard low-cost QTFs with resonance frequencies at 32.7 kHz have been employed in QEPAS sensors. The light source is focused between QTF prongs and sound waves produced by the modulated absorption of the gas are generated between the QTF prongs, forcing them to oscillate back and forth (in-plane anti-symmetrical flexural modes). The main problem in the realization of a QEPAS sensor is the focalization of the laser beam within the 300 μm-gap between the standard 32.7 kHz-QTF prongs without touching both micro-resonator tubes and the QTF itself. This is crucial in order to avoid the generation of a photo-thermal noise contribution which would be added to the piezoelectric signal [12-13]. When the light is periodically absorbed by the gas, the energy excess is mainly dissipated through non-radiative relaxation processes, involving vibrational and rotational excited states. Sound waves are then generated via energy transfer from excited states to translational degrees of freedom. The ability of the gas target to periodically relax the excess of energy depends on the modulation frequency (i.e. the resonance frequency of the QTF in-plane mode) of the incident laser radiation and differs for each gas. For slow relaxing gases, such as CO, $CO_2$ and NO, a frequency as high as 32.7 kHz can limit the sound wave generation efficiency [14-15]. When laser modulation occurs at one of resonance frequencies of in-plane piezoelectrically active modes, the induced strain field generates surface electric charges proportional to the intensity of the sound waves incident on the QTF prongs [16]. Therefore, all these considerations suggest directions for the realization of improved custom QTFs providing: i) a reduction of the QTF fundamental frequency while maintain a high the quality factor, ii) an increase of the prongs spacing in order to facilitate the optical alignments and minimize the

Quantum Sensing and Nano Electronics and Photonics XVI, edited by Manijeh Razeghi, Proc. of SPIE
Vol. 10926, 109260D · © 2019 SPIE · CCC code: 0277-786X/19/$18 · doi: 10.1117/12.2507932

photo-thermal noise level. Following these guidelines, custom QTFs have been successfully employed in QEPAS sensors [17-23].

In this work, we investigated the influence of prong sizes on both the resonance frequency and the quality factor of the fundamental flexural mode, leading to a QTF geometry designed to provide a fundamental mode resonance frequency of ~ 16 kHz, half of the resonance frequency of the standard 32 kHz-QTF, but with a quality factor as high as 15,000 at atmospheric pressure. Starting from this design, two novel QTF geometries were realized: the first with T-shaped prongs to optimize the strain field distribution between the prongs and their support and the latter having with grooves carved on the front and rear surface sides of each prong in order to increase the coupling between the electrodes and the resonance mode and consequentially reduce the QTF electrical resistance. QTFs were implemented in a QEPAS sensor and tested for the detection of a water vapor absorption line located at 1297.19 $cm^{-1}$.

## 2. NEW GENERATION OF QUARTZ TUNING FORKS

With the aim of determining the dependence of the resonance frequency and the related quality factor on the relevant QTF dimensions and identify the optimal design for QEPAS, a set of QTFs with different values of spacing between the prongs, their length and thickness as well as the crystal thickness was designed and tested, as reported in Ref. [24]. Even if the electro-elastic properties of QTFs are not influenced by the prong spacing (the two prongs can be assumed to be uncoupled), this parameter plays a crucial role in the acousto-electric transduction efficiency, i.e., the conversion efficiency of the amplitude of the acoustic wave in the piezoelectric charge production. For a focused laser beam, in the approximation of cylindrical symmetry, the amplitude of the acoustic wave incident on the prong surface decays as $1/\sqrt{g}$ [24], where $g$ is the distance of the QTF axis position from the internal prong surface. The size of the cross-sectional area of the focused beam is determined by diffraction to the beam waist values of the order of the laser wavelength. The larger the focused beam cross area-size, the larger has to be the prong spacing in order to avoid laser radiation hitting the QTF. For this reason, prongs spacings > 300 μm were investigated. In Ref. [24], the Euler-Bernoulli equation was used to predict the theoretical frequencies for the fundamental mode. An agreement within 10% of uncertainty between the experimental and theoretical frequency values was obtained, which confirms that it is possible to predict the resonance frequency of a QTF with a good accuracy. The results showed an empirical correlation between the quality factor and $Tw/L$ parameter ($L$, $w$ and $T$ are the prong length width and thickness, respectively), both at a pressure as low as 50 torr and atmospheric pressure, as reported in Fig. 1.

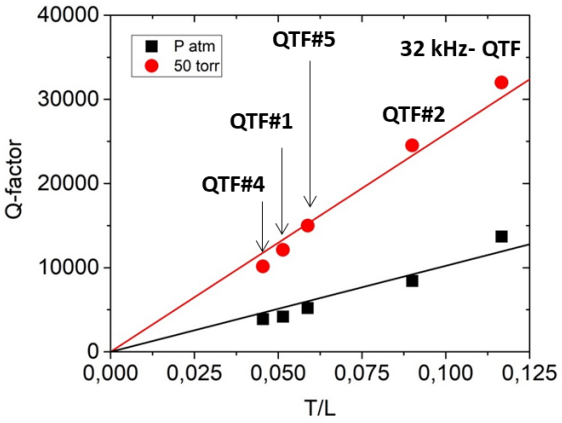


Figure 1. $Q$-factor values plotted as a function of the ratio between the prong thickness (T) and the prong (L), both at air pressure of 50 torr (red dot symbols) and atmospheric pressure (black square symbols). The QTF labels are the same as used in Ref. [24].

### 2.1 QTF-S08 and QTF-S15

For a novel generation of QTFs optimized for QEPAS operation, a resonance frequency of ~16 kHz (a half of the standard 32.7 kHz) was selected. By following the trend in Fig. 1 and combining it with the Euler-Bernoulli beam theory, at $f$ = 16 kHz, the $L$ and $T$ values (with $w$ = 0.25 mm) maximizing the quality factor are 9.4 mm and 2.0 mm, respectively. With this prong geometry two QTFs differing only in the prong spacing were designed: QTF-S08 having a

prong spacing of 0.8 mm, and QTF-S15 with a prong spacing of 1.5 mm. The design of QTF-S08 and QTF-S15 is depicted in Fig. 2.

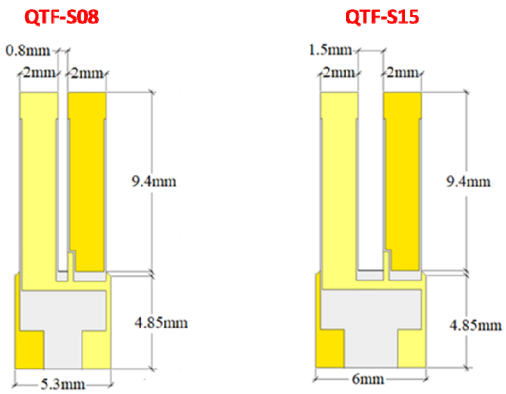


Figure 2. Schematic view of QTF-S08 and QTF-S15 sizes. The dark and light-yellow areas identify two different polarities of electrode gold pattern.

With all other geometrical parameters being identical, the influence of the prong spacing on the QTF frequency and Q-factor as well as on the QEPAS performance in terms of signal-to-noise ratio (SNR) can be performed.

### 2.2 T-QTF

When a QTF vibrates at its fundamental mode, the stress field is mainly localized at the junction between the prong base and the QTF support and it extends in the support area. In addition, in QEPAS the acoustic source is located between the prongs, close to the prongs top. This suggests that if some extra mass is added to the free end of the prong an increase of for the stress field intensity can be obtained. These considerations suggest modifying the prong geometry from the standard I-shape to a T-shape one. Starting from the prong geometry defined for QTF-S08, COMSOL Multiphysics was used to simulate the stress field distribution while the QTF is vibrating at its fundamental mode. The simulation shows that the T-shape results in a better distribution of the stress field associated with the vibration along the internal prong surface, where the generated charges are collected. A decrease of the resonance frequency of the fundamental mode is also predicted. The realized QTF geometry with T-shaped prong (T-QTF) that maximizes the stress field intensity is shown in Fig.3.

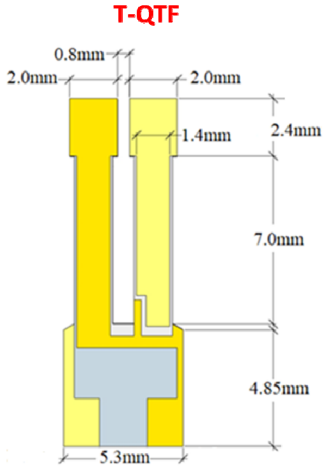


Figure 3. Schematic view of T-QTF sizes. The dark and light-yellow areas identify two different polarities of electrode gold pattern.

The prong thickness of 2.0 mm has been sharply reduced to 1.4 mm, starting from 2.4 mm from the prong top.

### 2.3 G-QTF

The trend reported in Fig. 1 combined with the Euler-Bernoulli beam theory leads to the prediction of a decrease of the quality factor while moving to lower resonance frequencies. A reduction of the quality factor causes an increase of the electrical resistance as reported in Refs. [24, 25]. Hence, it is convenient to keep the QTF electrical resistance at low values also for resonance frequencies lower than 32.7 kHz without affecting the quality factor. This can be achieved by carving rectangular grooves on both surface prongs. The QTF-S08 with grooves applied on both prongs is schematically shown in Fig. 4 and will be named hereafter as G-QTF.

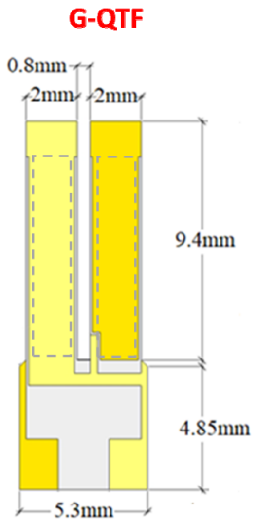


Figure 4. Schematic view of G-QTF sizes. Dashed areas represent grooves applied on both sides of QTF prongs. The dark and light-yellow areas identify two different polarities of electrode gold pattern.

These grooves were realized by carving 50 µm of the both crystal surfaces. The width of the areas placed between the grooves and the lateral edges of the prong was fixed at 100 µm.

## 3. CHARACTERIZATION OF QUARTZ TUNING FORKS

The electrical characterization of the QTF was performed by exciting the resonator electrically. A sinusoidal voltage excitation causes a charge displacement through the QTF prongs. The piezoelectric current is then converted to an output voltage by means of the trans-impedance amplifier and then the lock-in amplifier demodulates the signal at the same frequency as the waveform generator. The spectral response was fitted using a Lorentzian function to determine the peak resonance frequency, $f_0$, and the full-width-half-maximum value, $\Delta f$. Hence, the quality factor results $Q = f_0/\Delta f$. In Fig. 5, resonance frequencies, $Q$-factors and electrical resistance values of the investigated QTFs are reported. All measurements were performed in air at atmospheric pressure.

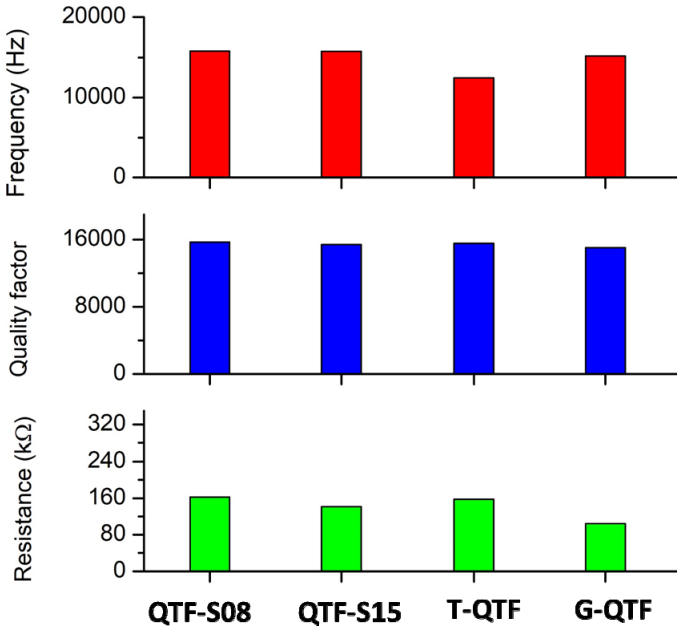


Figure 5. Resonance frequencies, quality factors and electrical resistance values measured for QTF-S08, QTF-S15, T-QTF and G-QTF, in air and at atmospheric pressure, are compared with those measured for QTF#5 at the first overtone mode and QTF#2 operating in the fundamental mode.

QTF-S08 and QTF-S15 share almost the same resonance frequency (15841.92 Hz and 15801.66, respectively) and Q-factor values (15710 and 15400, respectively), implying that the prong spacing does not affect the resonance properties of the QTF and thereby the two prongs can be considered almost uncoupled. G-QTF showed a resonance frequency (15222.93 Hz) ~ 620 Hz lower than QTF-S08, allowing to confirm that 50 μm-grooves carving on both surfaces slightly affects the rectangular geometry of the prong and produces a small shift of the resonance frequency. T-QTF has a resonance frequency (12460.55 Hz) significantly lower than that measured for QTF-S08, due to the non-uniformity of the moments of inertia along the prong section. However, it exhibits a quality factor of 15260, comparable to that measured for QTF-S08 and thus the T-geometry does not affect the quality factor. Moreover, T-shaping the prongs does not affect the electrical resistance, being nearly identical the electrical resistance measured for QTF-S08 (162.8 kΩ) and T-QTF (157.5 kΩ). Whereas, a comparison of QTF-S08 with G-QTF demonstrates that adding grooves on the prongs surfaces reduces the electrical resistance from 162.9 kΩ (QTF-S08) to 104.3 kΩ (G-QTF) while the Q-factor and resonance frequency are only slightly affected.

## 4. QEPAS PERFORMANCE

To test the QEPAS sensing performance, all investigated QTFs were used as a photoacoustic sensor in a QEPAS setup similar to that reported in Ref. [21]. A quantum cascade laser was used as the light source to detect the water vapor absorption line falling at 1297.19 $cm^{-1}$ with an intensity of $3.6 \cdot 10^{-22}$ cm/molecule. An aluminum enclosure equipped with two windows was realized in order to accommodate and easily exchange the QTFs. The housing was filled with standard air with a fixed 1.7% water vapor concentration at atmospheric pressure. In all QTFs, the laser beam was focused between the prongs, 2 mm from the QTF top. The QEPAS signals were acquired as a function of time while the laser frequency was locked to the selected water vapor absorption line peak. The results are reported in Fig. 6.

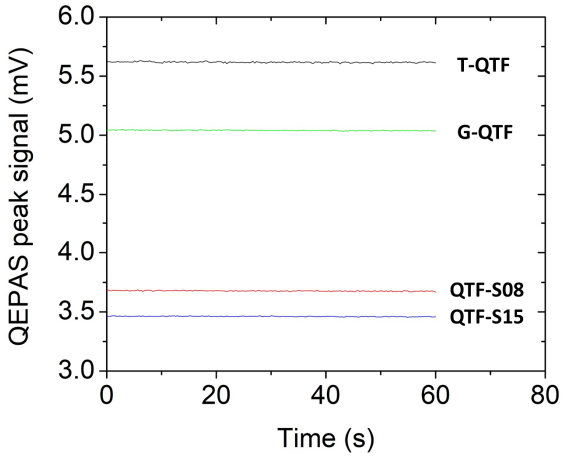

Figure 6. QEPAS signals as a function of time while the laser frequency is locked to the selected water absorption line peak.

The largest QEPAS signal was measured with the T-QTF (5.48 mV), about 1.5 times higher than that measured with QTF-S08 (3.68 mV). QTF-S08 provides a QEPAS signal about 6% higher than QTF-S15. This means that even if the resonance properties of QTFs (the resonance frequency, its quality factor and the electrical resistance) are not influenced by the prong spacing, this parameter can influence the QEPAS performance. G-QTF showed a QEPAS signal of 5.02 mV, 1.36 times higher than QTF-S08, demonstrating that even if the grooves on the prong surface slightly affect the resonance frequency and the *Q*-factor, a decrease of the electrical resistance is beneficial in terms of QEPAS performance.

## 5. T-QTF WITH A DUAL-TUBE RESONATOR SYSTEM

Among QTFs with a prong spacing of 0.8 mm, the T-QTF showed the best QEPAS performance. Hence, a T-QTF is the best candidate to be acoustically coupled with a pair of micro-resonator tubes, acting as amplifiers for the sound wave. The system composed by a QTF and resonator tubes is usually referred as a spectrophone. The T-QTF was positioned between the tubes to probe the acoustic vibration excited in the absorbing gas contained inside the tubes. The geometrical parameters influencing the sensor performance are: the internal diameter ID and the length *l* of the two tubes, together with the spacing between the tube and the surface of the QTF [3, 26-27]. A set of six different tubes with internal diameters ID = 1.36 mm, 1.41 mm, 1.52 mm, 1.59 mm, 1.83 mm and 2.06 mm, with lengths ranging from 10 to 15 mm, have been investigated. We experimentally verified that the QEPAS signal is maximized when both tubes with ID = 1.59 mm have a length of *l* =12.4 mm, both located 200 μm from the QTF prong surface. With such a spectrophone, the QEPAS scan of the water absorption line is shown in Fig. 7a, together with that obtained with a bare T-QTF (Fig. 7b).

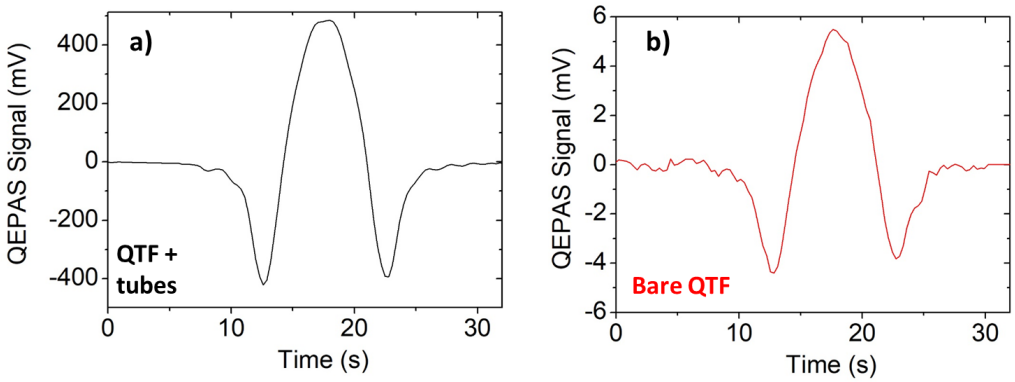

Figure 7. (a) QEPAS spectral scan of water absorption line acquired with the spectrophone composed of a T-QTF and a pair of micro-resonator tubes having a length of 12.4 mm and internal diameter of 1.59 mm, both positioned 200 μm from the QTF. (b) QEPAS spectral scan acquired with a bare T-QTF with the same experimental conditions.

The spectrophone showed a QEPAS peak signal of 482.6 mV, ~90 times higher than that measured with a bare T-QTF (5.48 mV). A corresponding SNR enhancement of ~ 60 was measured, which is a new record for mid-IR QEPAS spectroscopy.

## 6. CONCLUSIONS

In this work, we reported on the performance of a new generation of quartz tuning forks optimized for QEPAS operation. Starting from a QTF having a resonance frequency of 15.8 kHz and a quality factor of 15700 at atmospheric pressure, two novel prong geometry were investigated: a T-shaped prong and prongs with rectangular grooves carved on both surfaces. With a T-shaped prong geometry, the QTF resonance frequency was reduced to 12.4 kHz while the quality factor was not affected. When grooves were applied on both prongs, the electrical resistance was significantly reduced while the quality factor was not affected. All QTFs were employed as a photoacoustic sensor in a QEPAS setup for the detection of water vapor in the mid-infrared spectral range. The T-shaped QTF exhibited the highest QEPAS signal. Hence, it was selected to be acoustically coupled with a dual-tube micro-resonator system. Tubes having a length of 12.4 mm and an internal diameter of 1.59 mm, positioned about 200 μm far from the QTF surface, provide the highest SNR, ~ 60 times higher than that measured with a bare QTF.

## 7. ACKNOWLEDGMENTS

The authors from Dipartimento Interateneo di Fisica di Bari acknowledge financial support from THORLABS GmbH, within the joint research laboratory PolySense. Frank K. Tittel acknowledges support by the Welch Foundation under Grant No. C0568.

## REFERENCES

[1] Patimisco, P., Scamarcio, G., Tittel, F.K., Spagnolo, V., "Quartz-Enhanced Photoacoustic Spectroscopy: A Review," Sensors 14, 6165-6206 (2014).
[2] Sampaolo, A., Patimisco, P., Giglio, M., Vitiello, M.S., Beere, H.E., Ritchie. D.A., Scamarcio, G., Tittel, F. K., and Spagnolo, V., "Improved Tuning Fork for Terahertz Quartz-Enhanced Photoacoustic Spectroscopy," Sensors, 16, 439 (2016).
[3] Patimisco, P., Sampaolo, A., Zheng, H., Dong, L., Tittel, F.K. and Spagnolo V., "Quartz enhanced photoacoustic spectrophones exploiting custom tuning forks: a review," Adv. Phys. X 2, 169-187 (2016).
[4] Patimisco, P., Sampaolo, A., Dong, L., Tittel, F.K., Spagnolo V., "Recent advances in quartz enhanced photoacoustic sensing," Appl. Phys. Rev., 011106 (2018).
[5] Jahjah, M., Jiang, W., Sanchez, N.P., Ren, W., Patimisco, P., Spagnolo, V., Herndon, S.C., Griffin, R.J., and Tittel, F.K., "Atmospheric $CH_4$ and $N_2O$ measurements near Greater Houston area landfills using QCL-based QEPAS sensor system during DISCOVERY-AQ 2013," Opt. Lett. 39, 957-960 (2014).
[6] Sampaolo, A., Patimisco, P., Giglio, M., Chieco, L., Scamarcio, G., Tittel, F.K., and Spagnolo, V., "Highly sensitive gas leak detector based on a quartz-enhanced photoacoustic $SF_6$ sensor," Opt. Express 24, 15872-15881 (2016).
[7] Spagnolo, V., Patimisco, P., Pennetta, R., Sampaolo, A., Scamarcio, G., Vitiello, M.S., Tittel, F.K., "THz Quartz-enhanced photoacoustic sensor for $H_2S$ trace gas detection," Opt. Express 23, 7574-7582 (2015).
[8] Viciani, S., Siciliani de Cumis, M., Borri, S., Patimisco, P., Sampaolo, A., Scamarcio, G., De Natale, P., D'Amato, F., and Spagnolo, V., "A quartz-enhanced photoacoustic sensor for H2S trace-gas detection at 2.6 μm," Appl. Phys. B 119, 21-27 (2014).
[9] Sampaolo, A., Patimisco, P., Dong, L., Geras, A., Scamarcio, G., Starecki, T., Tittel, F. K., and Spagnolo, V., "Quartz-enhanced photoacoustic spectroscopy exploiting tuning fork overtone modes," Appl. Phys. Lett. 107, 231102 (2015).
[10] Giglio, M., Patimisco, P., Sampaolo, A., Scamarcio, G., Tittel, F. K., and Spagnolo, V., "Allan Deviation Plot as a Tool for Quartz-Enhanced Photoacoustic Sensors Noise Analysis," IEEE Trans. Ultrason. Ferroelect. Freq. Control, 63, 555-560 (2016).

[11] Patimisco, P., Sampaolo, A., Mackowiak, V., Rossmadl, H., Cable, A., Tittel, F.K., and Spagnolo, V., "Loss Mechanisms Determining the Quality Factors in Quartz Tuning Forks Vibrating at the Fundamental and First Overtone Modes," IEEE Trans. Ultrason. Ferroelect. Freq. Control, 65, 1951-1957 (2018).
[12] Dong, L., Spagnolo, V., Lewicki, R., and Tittel, F.K., "Ppb-level detection of nitric oxide using an external cavity quantum cascade laser based QEPAS sensor," Opt. Express 19, 24037-24045 (2011).
[13] Patimisco, P., Spagnolo, V., Vitiello, M. S., Tredicucci, A., Scamarcio, G., Bledt, C. M., and Harrington, J. A., "Coupling external cavity mid-IR quantum cascade lasers with low loss hollow metallic/dielectric waveguides," Appl. Phys. B 108, 255–260 (2012).
[14] Wysocki, G., Kosterev, A.A., and Tittel, F.K., "Influence of molecular relaxation dynamics on quartz-enhanced photoacoustic detection of $CO_2$ at $\lambda = 2$ μm," Appl. Phys. B 85, 301-306 (2006).
[15] Kosterev, A.A., Mosely, T.S., and Tittel, F.K., "Impact of humidity on quartz-enhanced photoacoustic spectroscopy based detection of HCN," Appl. Phys. B 85, 295–300 (2006).
[16] Patimisco, P., Sampaolo, A., Giglio, M., Mackowiak, V., Rossmadl, H., Gross, B., Cable, A., Tittel, F.K., and Spagnolo, V., "Octupole electrode pattern for tuning forks vibrating at the first overtone mode in quartz-enhanced photoacoustic spectroscopy," Opt. Lett. 43, 1854-1857 (2018).
[17] Zheng, H., Dong, L., Sampaolo, A., Wu, H., Patimisco, P., Yin, X., Ma, W., Zhang, L., Yin, W., Spagnolo, V., Jia, S., Tittel, F.K., "Single-tube on-beam quartz-enhanced photoacoustic spectroscopy," Opt. Lett. 41, 978-981 (2016).
[18] Zheng, H., Dong, L., Patimisco, P., Wu, H., Sampaolo, A., Yin, X., Li, S., Ma, W., Zhang, L., Yin, W., Xiao, L., Spagnolo, V., Jia, S., Tittel, F.K., "Double antinode excited quartz-enhanced photoacoustic spectrophone," Appl. Phys. Lett. 110, 021110 (2017).
[19] Wu, H., Yin, X., Dong, L., Pei, K., Sampaolo, A., Patimisco, P., Zheng, H., Ma, W., Zhang, L., Yin, W., Xiao, L., Spagnolo, V., Jia, S., Tittel, F.K., "Simultaneous dual-gas QEPAS detection based on a fundamental and overtone combined vibration of quartz tuning fork," Appl. Phys. Lett. 110, 121104 (2017).
[20] Zheng, H., Dong, L., Sampaolo, A., Wu, H., Patimisco, P., Ma, W., Zhang, L., Yin, W., Xiao, L., Spagnolo, V., Jia, S., and Tittel, F.K., "Overtone resonance enhanced single-tube on-beam quartz enhanced photoacoustic spectrophone," Appl. Phys. Lett. 109, 111103 (2016).
[21] Tittel, F.K., Sampaolo, A., Patimisco, P., Dong, L., Geras, A., Starecki, T., and Spagnolo, V., "Analysis of overtone flexural modes operation in quartz-enhanced photoacoustic spectroscopy," Opt. Express 24, A682-A692 (2016).
[22] Wang, Q., Wang, Z., Ren, W., Patimisco, P., Sampaolo, A., and Spagnolo, V., "Fiber-ring laser intracavity QEPAS gas sensor using a 7.2 kHz quartz tuning fork," Sensor Actuat. B-Chem. 227268, 512-518 (2018).
[23] Wu, H., Sampaolo, A., Dong, L., Patimisco, P., Liu, X., Zheng, H., Yin, X., Ma, W., Zhang, L., Yin, W., Spagnolo, V., Jia, S., and Tittel, F.K., "Quartz enhanced photoacoustic $H_2S$ gas sensor based on a fiber-amplifier source and a custom tuning fork with large prong spacing," Appl. Phys. Lett. 107, 111104 (2015).
[24] Patimisco, P., Sampaolo, A., Dong, L., Giglio, M., Scamarcio, G., Tittel, F.K., and Spagnolo, V., "Analysis of the electro-elastic properties of custom quartz tuning forks for optoacoustic gas sensing," Sensor Actuat. B-Chem. 227, 539-546 (2016).
[25] Hirata, M., Kokubun, K., Ono, M., and Nakayama, K., "Size effect of a quartz oscillator on its characteristics as a friction vacuum gauge," J. Vac. Sci. Technol. A 3, 1742-1745 (1985).
[26] Dong, L., Kosterev, A.A., Thomazy, D., Tittel, F.K., "QEPAS spectrophones: design, optimization, and performance," Appl. Phys. B 100, 627–635 (2010).
[27] Giglio, M., Patimisco, P., Sampaolo, A., Zifarelli, A., Blanchard, R., Pfluegl, C., Witinski, M.F., Vakhshoori, D., Tittel, F.K., and Spagnolo, V., Nitrous oxide quartz-enhanced photoacoustic detection employing a broadband distributed-feedback quantum cascade laser array," Appl. Phys. Lett. 113, 171101 (2018).